Published in final edited form as:
Magn Reson Med. 2009 August ; 62(2): 325–332. doi:10.1002/mrm.22011.

Relaxation effects of Ferucarbotran-labeled mesenchymal stem cells at 1.5T and 3T: Discrimination of viable from lysed cells

Tobias D Henning[1], **Michael F Wendland**[1], **Daniel Golovko**[2], **Elizabeth J Sutton**[1], **Barbara Sennino**[3], **Farbod Malek**[4], **Jan S Bauer**[2], **Donald M McDonald**[3], and **Heike Daldrup-Link**[1]

[1]Department of Radiology, UCSF Medical Center, University of California San Francisco, USA

[2]Department of Radiology, Technical University of Munich, Munich, Germany

[3]Department of Anatomy, UCSF, San Francisco, USA

[4]Department of Orthopedic Surgery, UCSF, San Francisco, USA

Abstract

Human mesenchymal stem cells (hMSC) were labeled with Ferucarbotran by simple incubation and cultured for up to 14 days. Iron content was determined by spectrometry and the intracellular localization of the contrast agent uptake was studied by electron and confocal microscopy. At various time points after labeling, reaching from 1 to 14 days, samples with viable or lysed labeled hMSCs, as well as non-labeled controls underwent MR imaging. SE- and GE-sequences with multiple TRs and TEs were used at 1.5T and 3T on a clinical scanner. Spectrometry showed an initial iron oxide uptake of 7.08 pg per cell. Microscopy studies revealed lysosomal compartmentalization. Contrast agent effects of hMSC were persistent for up to 14 days after labeling. A marked difference in the T_2-effect of compartmentalized iron oxides compared to free iron oxides was found on T_2-weighted sequences, but not on T_2*-sequences. The observed differences may be explained by the loss of compartmentalization of iron oxide particles, the uniformity of distribution and the subsequent increase in dephasing of protons on SE images. These results show that viable cells with compartmentalized iron oxides may – in principle – be distinguished from lysed cells or released iron oxides.

Keywords

Cell Labeling; Mesenchymal Stem Cells; MR Imaging; Ferucarbotran

Introduction

In recent years, stem cell research has provided insight into developmental biology, the origin of various diseases, and has initiated the development of numerous stem cell based therapeutic approaches (1–3). Among the various stem cell populations used for cell therapy, adult human mesenchymal stem cells (hMSCs) have been identified as ethical, practical and biologically acceptable cell populations for these purposes. They are easily derived from bone marrow aspirates, are efficiently expanded in vitro and can differentiate into a variety of specialized cell populations. In numerous animal and human studies, hMSCs have displayed excellent tissue regeneration potential (4,5). Treatment with hMSCs resulted in improved coronary perfusion in patients after acute myocardial infarction (5),

Corresponding author: Heike E Daldrup-Link M.D. PhD, Department of Radiology, 513 Parnassus Ave, San Francisco, CA 94143-0628, Ph.: (415)-476-2306, Fax: (415)-476-0616, Heike.Daldrup-Link@radiology.ucsf.edu.

cartilage repair in osteoarthritis (1) and favorable bone repair in patients with osteogenesis imperfecta (6). While these results paint a promising picture of stem cell based therapies, questions concerning the localization and viability of hMSCs post transplantation remain inadequately answered.

Labeling hMSCs with iron oxide based contrast agents allows for sensitive, non-invasive, real-time cell tracking *in vivo* via MR imaging (7–10). Various labeling methods and MR imaging techniques have been established for cell tracking *in vitro* (11–13), both in animal models (7,10,14) and in the clinical setting in patients (15). While most cell labeling studies to date concentrate on the anatomical localization of labeled stem cells (8), recent research attempts have focused on the functional aspects of transplanted cells, such as their viability (16), differentiation capacity (16,17) and long-term residence in the target organ (18,19). These aspects are essential for the assessment of successful stem cell based tissue regeneration.

Migration of transplanted stem cells from one location to another indicates unimpaired viability (19). However, if the cells stay at the site of local injection, for example in the case of hMSC transplantation into cartilage defects, additional criteria to verify the viability of the transplanted cells would be desirable. Recent studies suggest that iron oxides display different signal characteristics when concentrated inside cells versus in solution as free particles (20). These differences in MR signal intensities of intracellular and extracellular iron oxides may be explained by differences in their local concentration, their compartmentalization or their ability to interact with surrounding protons (21,22). Therefore, we hypothesize that this effect can be utilized to differentiate viable cells, which contain compartmentalized intracellular iron oxides, from non-viable cells, which have released iron oxides.

The purpose of this study was to investigate the differences in MR signal characteristics of viable versus dead hMSCs considering two major influencing variables: (1) the time point after the labeling process and (2) the applied field strength. Thus, we investigated the signal intensity of viable versus lysed, iron oxides labeled hMSC at (1) different time points after the labeling process and at (2) two different field strengths, 1.5 and 3 T.

Methods

Contrast Agent

Ferucarbotran (Resovist, Schering AG, Berlin, Germany) is a superparamagnetic iron oxide (SPIO) composed of a 4.2 nm crystalline nonstoichiometric Fe^{2+} and Fe^{3+} iron oxide core and a stabilizing carboxydextran coat. This coating ensures aqueous solubility and results in a net negative charge for the particle (23–25). The contrast agent has r_1 and r_2 relaxivities of $7.2 \pm 0.1\ mM^{-1}s^{-1}$ and $82.0 \pm 6.2\ mM^{-1}s^{-1}$ respectively (in blood at 37°C and 1.5 T) and a hydrodynamic diameter of 62 nm (25). Ferucarbotran is approved for MR imaging of the liver in patients in Europe since 2001 (24).

The size and the physicochemical surface properties of Ferucarbotran allow for efficient internalization into macrophages, monocytes and natural killer cells, without additional transfection agents (13,23,26). After uptake, the iron oxide particles are compartmentalized in endosomes and lysosomes within the cytoplasm of the cells (13).

Cell Culture

Human mesenchymal stem cells (hMSC) were obtained from a 20-year-old male donor without a bone marrow (BM) disorder, who was admitted to our institution for trauma surgery. The patient gave consent to donate BM via needle aspiration from the posterior iliac

crest. The study was approved by the Institutional Review Board. Preparation of hMSCs was done using slightly modified established protocols for primary cultures (27,28). BM mononuclear cells were plated in 100 cm^2 pretreated culture dishes (BD Falcon, Franklin Lakes, NJ, USA) and incubated overnight. Non-adherent cells were removed by washing. The remaining cells were grown in standard cell culture condition (37°C in a humidified 5% CO_2 atmosphere) using DMEM high glucose medium supplemented with 10% fetal bovine serum (FBS, Hyclone, Logan, UT) and 1% Penicillin-Streptomycin. Culture medium was changed every third day and the cells were split upon reaching 90% confluency. The stem cells were passaged no more than 12 times to preclude senescence.

Cell Labeling

For cell labeling, hMSCs were plated at 80% confluency and allowed to adhere overnight. The cell labeling solution, consisting of high glucose DMEM and Ferucarbotran at a concentration of 100 μg Fe/ml, was added to the cell culture flasks (100 μl/cm^2). After 2 hours of incubation in standard cell culture conditions, 10% FBS was added and cells were incubated for an additional 16 hours. Cells were typsinized, washed 3 times in PBS (25° C, 400 rcf, 5 min) and either replated or used for experiments. For proof of cell viability, a Trypan blue test was performed before and after all labeling procedures.

Before each MR experiment, cells were counted using a hemocytometer. For MR imaging, the cell samples were resuspended in 400 μl of isotonic Ficoll solution (density of 1.07 g/ml), which matches the density of hMSCs. The isodense Ficoll solution prevents cell sedimentation. Ficoll is widely used in the isolation of primary cultures, it preserves viability of the labeled cells during scanning (29,30).

First, reproducibility of the labeling efficiency was studied by labeling three cell cultures, each at three different time points relative to culture passages. The first triplicate was labeled at day 0, the second triplicate was labeled 6 days later and the third triplicate was labeled 12 days later. After measuring viability and cell count 0.5×10^5 cells were taken from each culture for iron content analysis by inductively coupled plasma atomic emission spectrometry (ICP-AES).

In the second experiment, a series of cell solutions were prepared in which 1×10^6 cells were taken from cultures that remained unlabeled or that were labeled 12, 10, 8, 6, 4, 3 and 1 day earlier, and placed in 0.4ml Ficoll (e.g. cell density of 2.5×10^6 cells/ml) for MRI. Identical series were prepared by adding 0.5×10^6, 0.25×10^6, 0.125×10^6 and 0.0625×10^6 cells in 0.4 ml Ficoll, yielding an array of 9 by 5 cell solutions with additional control solutions of Ficoll without cells. This experiment was performed to assess changes in iron content and MR relaxation over time during cell division and potential iron metabolism.

In a third experiment, all labeled cells were scanned at a specific time point (i.e. the cells labeled and their progeny). This should show if the iron content and MR signal characteristics of the whole cell population changed over time. For this, cells were labeled 14, 10, 4, 3, and 2 days prior to the experiment. Then, samples of these labeled cells and of unlabeled controls were lysed using a sonic dismembrator. Sonication causes physical disruption of cell membranes by pulsed, high frequency sound waves. Cells are lysed quickly and completely while no metabolism of contrast agent takes place. Sonication was performed at 20kHz for 90 seconds, intermittently sonicating and pausing in 5 second intervals, in order to avoid excessive heating of the sample (Sonic Dismembrator Model 100, Fisher Scientific, Pittsburgh, PA, USA). Finally, for MR imaging duplicates of 1.2×10^6 intact and lysed cells in 0.4 ml Ficoll from all the time points mentioned above were arranged in a tray and imaged.

MR Imaging and Data Analysis

All samples were scanned on clinical 1.5T and 3T MR scanners (Signa EXCITE HD 1.5T and Signa EXCITE HD 3T, GE Medical Systems, Milwaukee, WI, USA) using standard quadrature knee coils (Clinical MR Solutions, Brookfield, WI, USA). The test tubes were placed in a water-containing plastic container at room temperature (20°C) to minimize susceptibility artefacts from surrounding air. For measurements of T_1 and T_2 relaxation times, coronal spin echo (SE) sequences were obtained with multiple TR (250, 500, 1000 and 4000 ms) and TE (16, 32, 48 and 64 ms at 1.5T; 15, 30, 45, 60 ms at 3T) values. In addition, coronal gradient echo (GE) images were obtained with a flip angle of 30 degrees, a TR of 500 ms and varying TE values (3.7, 7.2, 14.4 and 28.8 ms). All sequences were acquired with a field of view (FOV) of 160×160 mm, a matrix of 256 × 196 pixels, a slice thickness of 5 mm and one acquisition.

MR images were transferred to DICOM format and processed by a self-written IDL program (Interactive Data Language, Research Systems, Boulder, CO, USA). T_1 and T_2-maps of the test samples were calculated by fitting the appropriate relaxation equation to the image data assuming monoexponential signal decay on a pixel-by-pixel basis. T_1 maps were calculated using SE sequences with a fixed TE (15 ms for 3 T, 16 ms for 1.5 T) and multiple TR values using the equation $M_z(t) = M0\ (1-\exp(-TR/T_1)$. T_2 maps were calculated from SE images obtained with TR 4000 ms and multiple TE values using the equation $M_{xy}(t) = M0\ \exp(-TE/T_2)$. T_2^* maps calculated from the GE images were inadequate due to low signal-to-noise, therefore T2* values were calculated from regions of interest (ROIs) selected from within the sample vials and the method of (31) was used to calculate T2* using the equation $M(TE)^2 = M0^2\exp(-2TE/T2^*)$. The relaxation times of intracellular iron oxides in viable cells were derived by ROI measurements of the test samples on calculated maps. SNR were derived by ROI measurements of the test samples on T_1, T_2 and T_2* images.

Iron content analysis

The iron concentration of all test samples was determined by inductively coupled plasma atomic emission spectrometry (ICP-AES). Samples were dissolved in a microwave by adding 65% HNO_3 and 30% H_2O_2. The obtained solutions were then nebulized into argon plasma. Collaborators from Schering AG Berlin, who were blinded with respect to the content of the samples, performed these analyses.

Confocal Microscopy

Labeled cells and unlabeled control cells were plated on glass chamber slides (Nunc, Rochester, NY, USA) and cultured as described above. Cells were fixed at 4°C with Carnoy's solution. Then, the dextran-coated iron oxides were stained by incubation with an anti-dextran FITC labeled antibody (Stem Cell Technologies, USA) at room temperature for 60 minutes. Finally, a DAPI-counterstain was performed (Vectashield, Vector, Burlingame, CA, USA) and the slides were mounted. Confocal microscopy was performed using a 40x objective (Zeiss LSM 510, Thornwood, NY, USA). Images were acquired using two different filters: for the DAPI staining a UV filter was used (wavelength 351 nm); for the FITC staining an Argon/2 filter was used (wavelength 488 nm).

Electron Microscopy

Adherent cell cultures grown on Thermanox coverslips were fixed with 2% glutaraldehyde in 0.1M sodium cacodylate buffer, postfixed with 1% osmium tetroxide followed by 2% aqueous uranyl acetate. The samples were dehydrated with ethanol and embedded in epoxy resin. Ultrathin sections were stained with 2% uranyl acetate and Reynolds lead-citrate.

They were examined and photographed at 80kV in a JEOL 100CX II (Jeol, Peabody, MA, USA).

Statistical Analysis

The experiment to assess the reproducibility of labeling efficiency was performed in triplicate, the comparison of lysed and viable cells was performed in quadruples. Quantitative data from these studies were compared between different groups of cells (e.g. before and after cell labeling, viable and non-viable cells) for significant differences with a t-test and a p-value of less than 0.05. To lower the multiple testing problem, repeated pairwise comparisons in one sample were adjusted with the Bonferroni correction. Statistical computation was done using SPSS 17.0 software (Munich, Germany).

Results

Cell Labeling and reproducibility of labeling

Analysis of iron content in labeled hMSCs found reproducible cellular iron uptake, with 7.08 ± 0.48 pg iron per cell after the labeling process. The iron content in unlabeled cells was under the detection limit of the equipment used (Figure 1). This represents a labeling efficiency (amount of iron internalized by cells divided by amount of iron in labeling media) of 0.52% ± 0.074%. No significant reduction in labeling efficiency was evident for cells labeled 6 or 12 days apart from that (Figure 1, $p > 0.05$). Examination of cells by fluorescence microscopy immediately after labeling and four weeks after labeling showed that the contrast agent was located predominantly inside the cells, with very few iron oxide particles localized at the cell membrane or outside of the cell (Figure 2, a – c). Electron microscopy of labeled cells confirmed intracellular distribution and showed Ferucarbotran particles in lysosomal compartments within the cytoplasm of the cell (Figure 2, d – f). After sonication, the cellular compartmentalization was destroyed and contrast agent was released (Figure 2 g).

Moreover, the cellular structure of labeled cells showed no noticeable morphologic abnormalities when compared to unlabeled controls on fluorescence microscopy or electron microscopy. In addition the labeled cells showed a doubling time of approximately 7 days, which was not significantly different from unlabeled cells. Trypan blue exclusion testing before and after the labeling process showed no significant difference in viability between different samples of labeled cells versus non-labeled controls. All samples exhibited viabilities greater than 97% and the viability of labeled cells did not change significantly at different time points after labeling (Figure 1).

Timecourse of iron content and MRI relaxation

Cell solutions prepared in sample vials containing 1×10^6 cells and serial dilutions down to 6.25×10^4 cells in 0.4mL Ficoll at various time points up to 12 days after labeling were evaluated. ICP-AES showed an initial iron oxide content of 7.07 pg per cell at day 1, followed by a moderate decline in samples for cells labeled multiple days prior to analysis (Figure 3). Corresponding MR studies showed an initial decrease of T_2 relaxation times (e.g. increased R_2) of labeled cells compared to unlabeled controls followed by a modest increase toward baseline value over the observation period of 12 days consistent with the measured decrease in iron content (Figure 3). In addition, the change in T_2 values decreased as expected for serially diluted cells, with a marked change from control evident for the most dilute cell solution (62.5×10^4 cells in 0.4mL). These data were consistent at 1.5 and at 3T. T_2* values could be measured only for the most dilute labeled cell solutions due to large signal reductions at even the smallest TE values. T_2* of cell solution at day 1 was 8.9 ± 1.6ms, substantially reduced from T_2* of 24.4 ± 2.5ms observed for unlabeled cells.

Moreover the reduction of T_2 effects over time post labeling was not evident in measured T_2* values, instead no marked effect of time was observed. T_1 relaxation times at the same cell dilution showed an initial decrease from unlabeled controls (T_1 = 1481 ms) to labeled cells (T_1 = 1219 ms) at day 1. As it was found for T_2* relaxation times, these values showed no marked effect over the timecourse of 12 days (T_1 = 1208 ms.)

In the second experimental setup, which included all progenies, disruption of cells by sonication to maximally release the internalized SPIO caused great reduction in signal on all SE images. It was not possible to evaluate either T_2 or T_1 for these solutions because MRI signal of all sonicated cell solutions was at noise level using minimal TE setting. The T_2* values of disrupted cell solution were reduced to 3.9 ± 0.3 ms, slightly less than half of intact cell solutions. Therefore, we compared the signal to noise ratios (SNR, Figure 4) for viable and lysed samples based on T_1, T_2 and T_2* sequences. Viable cells showed significantly higher SNRs on T_1 and T_2-weighted SE sequences compared to released iron oxides. On the other hand, differences in SNR-data on T_2*-weighted sequences were only minimal and not significantly different. The differences in SNR data of compartmentalized iron oxides in viable cells and released iron oxides from lysed cells were slightly more pronounced at 3T than at 1.5T (Figure 4). In the second experimental setup, which included all progenies, the iron content of the whole samples did not decrease significantly ($p > 0.05$).

At both, 1.5T and at 3T, the samples with viable labeled cells displayed markedly greater MR signal when compared to samples with lysed labeled cells, from which iron oxide particles would be liberated (Figure 5, images acquired at 3T). Viable Ferucarbotran-labeled cells showed a T_2-effect on our moderately T_2-weighted SE sequences while the same quantity of free iron oxides, that had been released from lysed cells, showed a markedly stronger T_2-effect. Major signal reduction on SE images was also observed for short echo times as used on T_1 sequences (Figure 4 and Figure 5).

Discussion

Our data showed that (a) labeling hMSCs with Ferucarbotran at the level of roughly 7pg iron/cell did not attenuate viability of the cells over 12 days post labeling; (b) the amount of iron oxide taken up by the cells was reproducible over multiple labeling procedures; (c) the quantity of iron oxide inside single cells declined as the cells divided, but the total intracellular iron of all progeny was not diminished over this time; (d) substantial Ferucarbotran-induced effects on MR relaxation of hMSC solutions were evident up to 14 days after labeling; and (e) sonication-induced cell lysis of viable cells to disperse the internalized Ferucarbotran caused a marked decline in MRI signal intensity and increase in T_2-relaxation rate. In our in vitro study, this effect could be used to differentiate intracellular iron oxides in viable cells from iron oxides, which had been released from lysed cells.

The large reduction in MRI signal intensity caused by disruption of cells and liberation of incorporated SPIO particles implies a big change in T2 relaxivity for extracellular versus intracellular particles. It is well known that relaxivity of susceptibility contrast materials is highly dependent on geometry and microscopic distribution of the magnetic centers. The observed differences on SE T_2- versus GE T_2*-weighted images in our study may be explained by many iron oxide particles being sequestered inside a few cells. Upon lysis of the cells the iron oxide particles disperse more uniformly throughout the sample causing a substantial reduction in distance between iron oxide particles. Using nominal density of 5.1 g/ml for iron oxide, iron fractional mass of approximately 72% and assuming a 4.2 nm sphere diameter for the iron oxide crystal in Ferucarbotran, we have an estimated iron mass of 1.43×10^{-19} g per crystal. Since the iron assay yielded approximately 7 pg of Fe loaded into each cell, we estimate roughly 4.9×10^{7} crystals per cell. We do not know how many

crystals comprise each SPIO particle, but if there are 8–10 crystals per particle it is still possible that distance between superparamagnetic centers, which would be proportional to the cubed root of the number of particles, may be reduced by roughly hundred-fold as a consequence of cellular disruption. Consequently an increased fraction of water molecules would be close to steep field gradients near the particles and would visit microscopic regions of the inhomogeneous magnetic field while diffusing during the TE interval.

On the other hand, the T_2* weighted images could exhibit much less effect upon disruption because the static field inhomogeneity would be less altered by cell disruption (22,32). For example, if only a few very large magnetic particles were internalized into each cell, one would not expect to detect any change on T_2 weighted SE images upon cell disruption. The observed signal characteristics are in accordance with previous studies: Simon et al. found increased R_1 and R_2-values for free versus intracellularly compartmentalized USPIO in vitro (20). In that study, monocytes were labeled with Ferumoxides USPIO particles and the cellular iron content was 10-fold less than the labeled hMSCs used in the current study. The difference in iron labeling can be attributed to a combination of factors including that monocytes are physically smaller cells than hMSCs, greater uptake efficiency for larger SPIO versus USPIO, and a larger per-particle iron content for SPIOs versus USPIOs. However the cell solutions used in the study of Simon et al contained roughly 10-fold more cells than the current study, so the total iron content of the cell solutions were similar. Yet in the former study uncompartmentalized USPIOs caused an increase of T_1- and T_2relaxation rates in comparison to intracellular USPIO, while in the current study disruption of cells containing SPIOs caused an overwhelming T_2–effect that severely attenuated signal, such that T_2 and T_1 could not be evaluated and their relaxation rates could not be measured. In addition, Tanimoto et al. showed in vivo that R_2* effects can be evoked by clustering of iron oxides, which would be comparable to the effect evoked by compartmentalization (33). To our knowledge, this is the first study that applies this effect for the differentiation of viable and lysed cells.

We found that the described different T_2-signal characteristics of iron oxides in viable cells and iron oxides released from dead cells were consistently observed (A) at different time points over 14 days and (B) at two different field strengths, 1.5 T and 3T.

Within the 14-day observation period, we found consistently different signal characteristics of intracellular iron oxides and free iron oxides. It can be deduced that neither iron oxide metabolization nor cell proliferation altered this effect. The cellular iron content and T_2-effect stayed nearly constant for the whole proliferating cell population and slowly decreased for individual cells. This can be explained by a distribution and dilution of the internalized iron oxides in proliferating progenies and minimal or absent metabolization of the contrast agent for up to 14 days after labeling. The positive staining for the dextran coat of the iron oxides for up to 4 weeks after labeling further supports the conclusion that no major metabolism of the contrast agent particles occurred during our experiment (Figure 2). Other authors described that they found a persistent T_2-effect of iron oxide labeled mesenchymal stem cells in vivo 7 days after localized injection in the myocardium (34) or in the kidney after injection into the renal artery (9). Even after injection of highly proliferative neural stem cells detection was possible for up to 32 days (35). However, Walczak et al reported that the proliferation-induced dilution of the contrast agent in cell lines with a high rate of proliferation - neural stem cells in that case - limits the long-term detectability by MR imaging (36). In slowly proliferating cell types like the mesenchymal stem cells used in this study, this effect should not affect the detectability.

Studies with longer follow up intervals showed that iron oxides are slowly metabolized within the lysosomes and incorporated into the body’s iron metabolism (37). Arbab and

coworkers reported, that the intracellular iron oxide metabolization is dependent on the contrast agent type, the applied labeling technique and the pH of the cells cytoplasm (38). All these discussed mechanisms, cell proliferation, dilution in progenies, iron metabolization, and potential cellular iron elimination, are expected to result in a slow decline in cellular iron content, and consequently, a decline in the cells T_2-signal effect over time. We hypothesize, that any increase in T_2-effect at the transplantation site after local transplantation of labeled cells would be an indicator of iron oxides release and cell death.

Another important factor for potential in vivo applications will be the proton density and proton diffusion capacity within the target organ. Since the observed T_2-effects are apparently dependent on the degree of interaction between protons and iron oxides, our results are more likely reproducible in vivo in a proton-rich pathology (e.g. edema) than in a proton-deprived environment.

In vivo applications of our technique are also dependent on additional biologic factors. Our technique to differentiate viable and dead cells is based on differences in T_2-effects and dependent on a lysis and iron release of dying cells. There are two major mechanisms how cell death can occur – necrosis and apoptosis (39). Necrosis results in cell lysis and subsequent inflammatory response (40). It is to be expected that processes resulting in necrosis and cell lysis will produce a similar signal behavior as we have shown. On the other hand, apoptosis is a regulated cell death where controlled degradation occurs leading to fragmentation of the cell. This type of cell death will result in the same iron content being compartmentalized among many cell fragments. This would be similar to the behavior seen in our scans with increasing cell counts – the R_2 relaxation rate would be the parameter most sensitive to change in this case. In many instances, both mechanisms may be involved after cell transplantation.

In addition, necrotic or apoptotic cells as well as released iron oxide particles may undergo a secondary phagocytosis by macrophages. The relation between the number of lysed cells and the number of macrophages would determine the resulting rate of compartmentalization and thereby a possible contrast agent effect. Therefore, the consistency of the surrounding tissue (fluid necrosis vs solid scar tissue) in which the release and the re-compartmentalization of iron oxide particles takes place and the number of macrophages will determine the possibility to detect a graft failure. Thus *in vivo* applications will be more complex and will have to evaluate various different pathologies in order to clarify, if the results from our *in vitro* model are applicable for certain pathologies and target organs in vivo.

Conclusion

In conclusion, our in vitro data show a persistent contrast agent effect and an increase in T_2-relaxation rate induced by cell lysis. In our in vitro study, this effect could be used to differentiate intracellular iron oxides in viable cells from iron oxides, which had been released from lysed cells. If these results could be applied in vivo, it would allow for a non-invasive diagnosis of a treatment failure after hMSC transplantation. An increased T2-effect at the transplantation site would then be indicative of graft failure.

Acknowledgments

This work was supported by a seed grant from the Department of Radiology, University of California of San Francisco. Tobias D Henning was supported by a research stipend from the German Research Association (DFG, HE 4578/1).

Literature

1. Caplan AI. Review: mesenchymal stem cells: cell-based reconstructive therapy in orthopedics. Tissue Eng. 2005; 11(7–8):1198–1211. [PubMed: 16144456]
2. Freed CR, Greene PE, Breeze RE, Tsai WY, DuMouchel W, Kao R, Dillon S, Winfield H, Culver S, Trojanowski JQ, Eidelberg D, Fahn S. Transplantation of embryonic dopamine neurons for severe Parkinson's disease. N Engl J Med. 2001; 344(10):710–719. [PubMed: 11236774]
3. Soria B, Roche E, Berna G, Leon-Quinto T, Reig JA, Martin F. Insulin-secreting cells derived from embryonic stem cells normalize glycemia in streptozotocin-induced diabetic mice. Diabetes. 2000; 49(2):157–162. [PubMed: 10868930]
4. Gregory CA, Prockop DJ, Spees JL. Non-hematopoietic bone marrow stem cells: molecular control of expansion and differentiation. Exp Cell Res. 2005; 306(2):330–335. [PubMed: 15925588]
5. Chen SL, Fang WW, Ye F, Liu YH, Qian J, Shan SJ, Zhang JJ, Chunhua RZ, Liao LM, Lin S, Sun JP. Effect on left ventricular function of intracoronary transplantation of autologous bone marrow mesenchymal stem cell in patients with acute myocardial infarction. Am J Cardiol. 2004; 94(1):92–95. [PubMed: 15219514]
6. Horwitz EM, Prockop DJ, Fitzpatrick LA, Koo WW, Gordon PL, Neel M, Sussman M, Orchard P, Marx JC, Pyeritz RE, Brenner MK. Transplantability and therapeutic effects of bone marrow-derived mesenchymal cells in children with osteogenesis imperfecta. Nat Med. 1999; 5(3):309–313. [PubMed: 10086387]
7. Jain M, Pfister O, Hajjar RJ, Liao R. Mesenchymal stem cells in the infarcted heart. Coron Artery Dis. 2005; 16(2):93–97. [PubMed: 15735401]
8. Hauger O, Frost EE, van Heeswijk R, Deminiere C, Xue R, Delmas Y, Combe C, Moonen CT, Grenier N, Bulte JW. MR evaluation of the glomerular homing of magnetically labeled mesenchymal stem cells in a rat model of nephropathy. Radiology. 2006; 238(1):200–210. [PubMed: 16373768]
9. Bos C, Delmas Y, Desmouliere A, Solanilla A, Hauger O, Grosset C, Dubus I, Ivanovic Z, Rosenbaum J, Charbord P, Combe C, Bulte JW, Moonen CT, Ripoche J, Grenier N. In vivo MR imaging of intravascularly injected magnetically labeled mesenchymal stem cells in rat kidney and liver. Radiology. 2004; 233(3):781–789. [PubMed: 15486216]
10. Unger EC. How can superparamagnetic iron oxides be used to monitor disease and treatment? Radiology. 2003; 229(3):615–616. [PubMed: 14657295]
11. Walczak P, Ruiz-Cabello J, Kedziorek DA, Gilad AA, Lin S, Barnett B, Qin L, Levitsky H, Bulte JW. Magnetoelectroporation: improved labeling of neural stem cells and leukocytes for cellular magnetic resonance imaging using a single FDA-approved agent. Nanomedicine. 2006; 2(2):89–94. [PubMed: 17292120]
12. Frank JA, Anderson SA, Kalsih H, Jordan EK, Lewis BK, Yocum GT, Arbab AS. Methods for magnetically labeling stem and other cells for detection by in vivo magnetic resonance imaging. Cytotherapy. 2004; 6(6):621–625. [PubMed: 15773025]
13. Metz S, Bonaterra G, Rudelius M, Settles M, Rummeny EJ, Daldrup-Link HE. Capacity of human monocytes to phagocytose approved iron oxide MR contrast agents in vitro. Eur Radiol. 2004; 14(10):1851–1858. [PubMed: 15249981]
14. Heyn C, Ronald JA, Mackenzie LT, MacDonald IC, Chambers AF, Rutt BK, Foster PJ. In vivo magnetic resonance imaging of single cells in mouse brain with optical validation. Magn Reson Med. 2006; 55(1):23–29. [PubMed: 16342157]
15. de Vries IJ, Lesterhuis WJ, Barentsz JO, Verdijk P, van Krieken JH, Boerman OC, Oyen WJ, Bonenkamp JJ, Boezeman JB, Adema GJ, Bulte JW, Scheenen TW, Punt CJ, Heerschap A, Figdor CG. Magnetic resonance tracking of dendritic cells in melanoma patients for monitoring of cellular therapy. Nat Biotechnol. 2005; 23(11):1407–1413. [PubMed: 16258544]
16. Arbab AS, Yocum GT, Rad AM, Khakoo AY, Fellowes V, Read EJ, Frank JA. Labeling of cells with ferumoxides-protamine sulfate complexes does not inhibit function or differentiation capacity of hematopoietic or mesenchymal stem cells. NMR Biomed. 2005; 18(8):553–559. [PubMed: 16229060]

17. Kostura L, Kraitchman DL, Mackay AM, Pittenger MF, Bulte JW. Feridex labeling of mesenchymal stem cells inhibits chondrogenesis but not adipogenesis or osteogenesis. NMR Biomed. 2004; 17(7):513–517. [PubMed: 15526348]

18. Yang L, Xia Y, Zhao H, Zhao J, Zhu X. Magnetic resonance imaging of transplanted neural stem cells in Parkinson disease rats. J Huazhong Univ Sci Technolog Med Sci. 2006; 26(4):489–492. [PubMed: 17120757]

19. Shapiro EM, Gonzalez-Perez O, Manuel Garcia-Verdugo J, Alvarez-Buylla A, Koretsky AP. Magnetic resonance imaging of the migration of neuronal precursors generated in the adult rodent brain. Neuroimage. 2006; 32(3):1150–1157. [PubMed: 16814567]

20. Simon GH, Bauer J, Saborovski O, Fu Y, Corot C, Wendland MF, Daldrup-Link HE. T1 and T2 relaxivity of intracellular and extracellular USPIO at 1.5T and 3T clinical MR scanning. Eur Radiol. 2006; 16(3):738–745. [PubMed: 16308692]

21. Majumdar S, Zoghbi SS, Gore JC. The influence of pulse sequence on the relaxation effects of superparamagnetic iron oxide contrast agents. Magn Reson Med. 1989; 10(3):289–301. [PubMed: 2733587]

22. Weisskoff RM, Zuo CS, Boxerman JL, Rosen BR. Microscopic susceptibility variation and transverse relaxation: theory and experiment. Magn Reson Med. 1994; 31(6):601–610. [PubMed: 8057812]

23. Daldrup-Link HE, Meier R, Rudelius M, Piontek G, Piert M, Metz S, Settles M, Uherek C, Wels W, Schlegel J, Rummeny EJ. In vivo tracking of genetically engineered, anti-HER2/neu directed natural killer cells to HER2/neu positive mammary tumors with magnetic resonance imaging. Eur Radiol. 2005; 15(1):4–13. [PubMed: 15616814]

24. Reimer P, Balzer T. Ferucarbotran (Resovist): a new clinically approved RES-specific contrast agent for contrast-enhanced MRI of the liver: properties, clinical development, and applications. Eur Radiol. 2003; 13(6):1266–1276. [PubMed: 12764641]

25. Wang YX, Hussain SM, Krestin GP. Superparamagnetic iron oxide contrast agents: physicochemical characteristics and applications in MR imaging. Eur Radiol. 2001; 11(11):2319–2331. [PubMed: 11702180]

26. Simon GH, von Vopelius-Feldt J, Fu Y, Schlegel J, Pinotek G, Wendland MF, Chen MH, Daldrup-Link HE. Ultrasmall supraparamagnetic iron oxide-enhanced magnetic resonance imaging of antigen-induced arthritis: a comparative study between SHU 555 C, ferumoxtran-10, and ferumoxytol. Invest Radiol. 2006; 41(1):45–51. [PubMed: 16355039]

27. Kassem M, Mosekilde L, Eriksen EF. 1,25-dihydroxyvitamin D3 potentiates fluoride-stimulated collagen type I production in cultures of human bone marrow stromal osteoblast-like cells. J Bone Miner Res. 1993; 8(12):1453–1458. [PubMed: 8304046]

28. Wang ML, Nesti LJ, Tuli R, Lazatin J, Danielson KG, Sharkey PF, Tuan RS. Titanium particles suppress expression of osteoblastic phenotype in human mesenchymal stem cells. J Orthop Res. 2002; 20(6):1175–1184. [PubMed: 12472226]

29. Graziani-Bowering GM, Graham JM, Filion LG. A quick, easy and inexpensive method for the isolation of human peripheral blood monocytes. J Immunol Methods. 1997; 207(2):157–168. [PubMed: 9368642]

30. Pittenger MF, Mackay AM, Beck SC, Jaiswal RK, Douglas R, Mosca JD, Moormann MA, Simonetti DW, Craig S, Marshak DR. Multilineage potential of adult human mesenchymal stem cells. Science. 1999; 284(5411):143–147. [PubMed: 10102814]

31. Miller AJ, Joseph PM. The use of power images to perform quantitative analysis on low SNR MR images. Magn Reson Imaging. 1993; 11(7):1051–1056. [PubMed: 8231670]

32. Bowen CV, Zhang X, Saab G, Gareau PJ, Rutt BK. Application of the static dephasing regime theory to superparamagnetic iron-oxide loaded cells. Magn Reson Med. 2002; 48(1):52–61. [PubMed: 12111931]

33. Tanimoto A, Oshio K, Suematsu M, Pouliquen D, Stark DD. Relaxation effects of clustered particles. J Magn Reson Imaging. 2001; 14(1):72–77. [PubMed: 11436217]

34. Kraitchman DL, Heldman AW, Atalar E, Amado LC, Martin BJ, Pittenger MF, Hare JM, Bulte JW. In vivo magnetic resonance imaging of mesenchymal stem cells in myocardial infarction. Circulation. 2003; 107(18):2290–2293. [PubMed: 12732608]

35. Magnitsky S, Watson DJ, Walton RM, Pickup S, Bulte JW, Wolfe JH, Poptani H. In vivo and ex vivo MRI detection of localized and disseminated neural stem cell grafts in the mouse brain. Neuroimage. 2005; 26(3):744–754. [PubMed: 15955483]

36. Walczak P, Kedziorek DA, Gilad AA, Barnett BP, Bulte JW. Applicability and limitations of MR tracking of neural stem cells with asymmetric cell division and rapid turnover: the case of the shiverer dysmyelinated mouse brain. Magn Reson Med. 2007; 58(2):261–269. [PubMed: 17654572]

37. Weissleder R, Cheng HC, Bogdanova A, Bogdanov A Jr. Magnetically labeled cells can be detected by MR imaging. J Magn Reson Imaging. 1997; 7(1):258–263. [PubMed: 9039625]

38. Arbab AS, Wilson LB, Ashari P, Jordan EK, Lewis BK, Frank JA. A model of lysosomal metabolism of dextran coated superparamagnetic iron oxide (SPIO) nanoparticles: implications for cellular magnetic resonance imaging. NMR Biomed. 2005; 18(6):383–389. [PubMed: 16013087]

39. Krysko DV, D'Herde K, Vandenabeele P. Clearance of apoptotic and necrotic cells and its immunological consequences. Apoptosis. 2006; 11(10):1709–1726. [PubMed: 16951923]

40. Festjens N, Vanden Berghe T, Vandenabeele P. Necrosis, a well-orchestrated form of cell demise: signalling cascades, important mediators and concomitant immune response. Biochim Biophys Acta. 2006; 1757(9–10):1371–1387. [PubMed: 16950166]

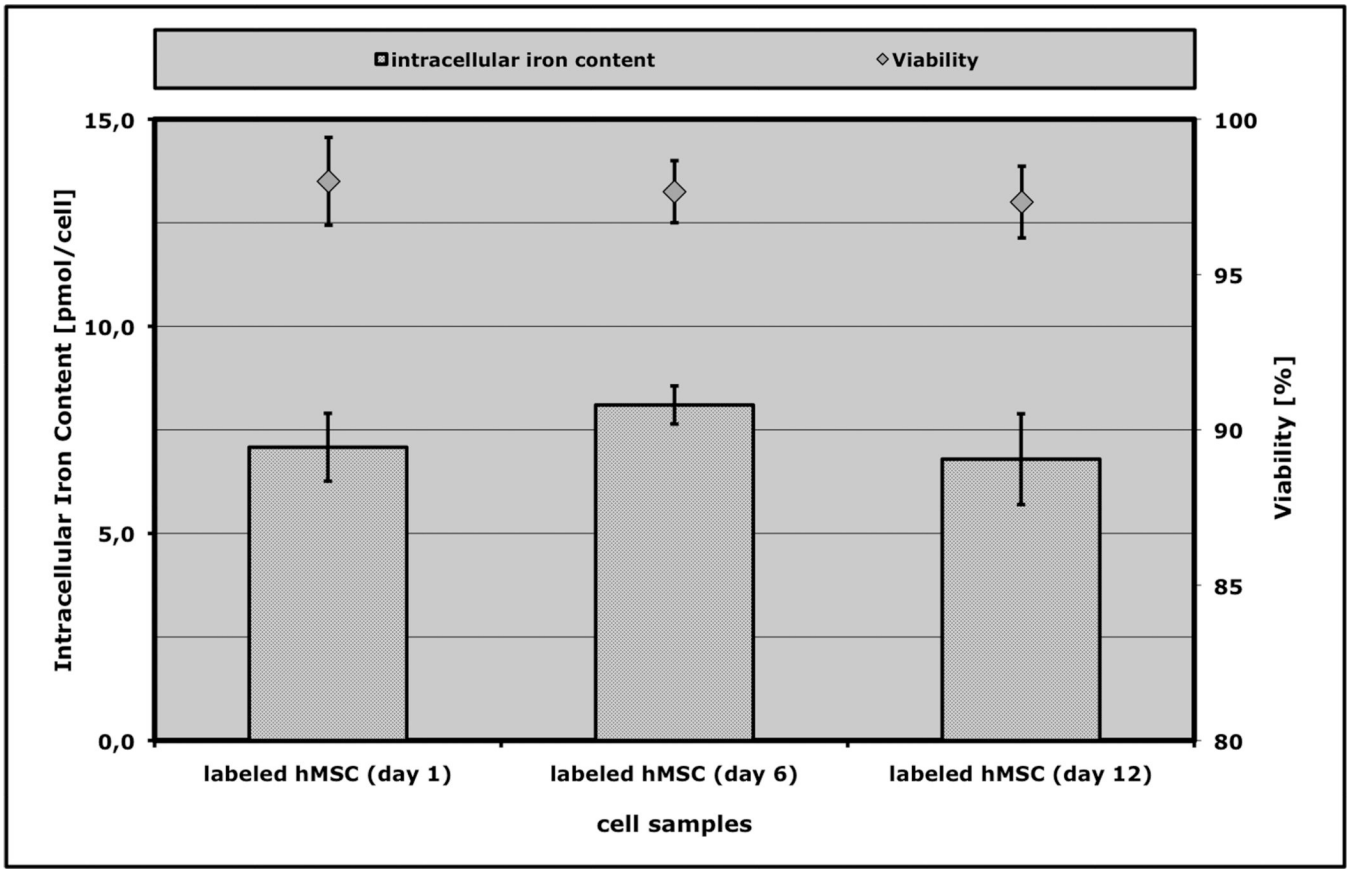

Figure 1.
Reproducibility of labeling efficiency over time. Data are displayed as mean data and standard deviations of the iron content and of the viability of hMSCs after incubation with Ferucarbotran (n=3 in each group). The cell samples labeled in different experiments (each 6 days apart from each other) do not show significant differences in iron oxide uptake or cell viability.

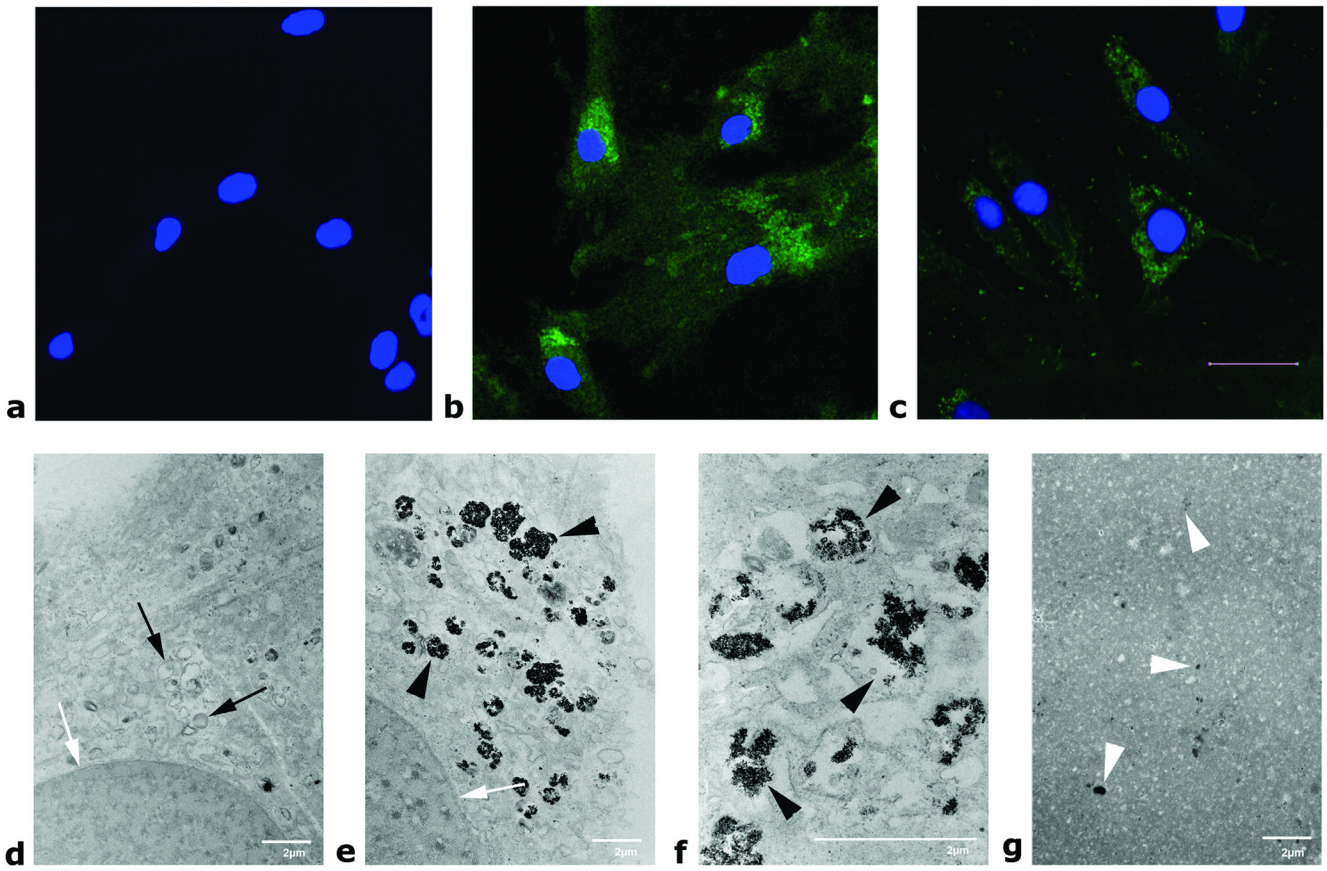

Figure 2.

Upper row: Confocal microscopy of unlabeled hMSC (a) as well as 1 day (b) and 4 weeks (c) after labeling with Ferucarbotran. Cells were stained with an anti-dextran FITC antibody (green) and the nucleus was counterstained with DAPI (blue). Four weeks after labeling, the dextran coating of the contrast agent particles could still be stained. The stronger staining immediately after labeling (b) suggests a higher intracellular concentration of the contrast agent particles. Scale bar corresponds to 20 µm. Lower row: Electron microscopy of hMSC: Unlabeled controls (d, 4100×), labeled hMSC (e, 4100× and f, 12500×) showing the contrast agent within lysosomes, lysed hMSC (g, 3600×, diluted 1:10 in gelatin). White arrows indicate the nucleus; black arrows show normal lysosomes; black arrowheads show contrast agent filled lysosomes. Note the total absence of intracellular compartments and the even distribution of free contrast agent after cell lysis in g (white arrowheads). Scale bars correspond to 2µm.

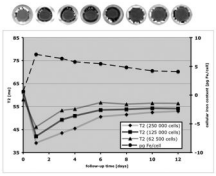

Figure 3.
T_2 map (top), intracellular iron content (dotted line) and T_2 times of labeled cells (solid lines) over a time period of 12 days as acquired at 3T. The images of the T2 maps correspond to the time points as indicated in the graph. Note, that the labeled hMSC still contain 4.1 pg Fe/cell after 12 days. The contrast agent effect and the decrease over the observed time period could be seen in both, T_2 maps as well as in the corresponding T_2 times.

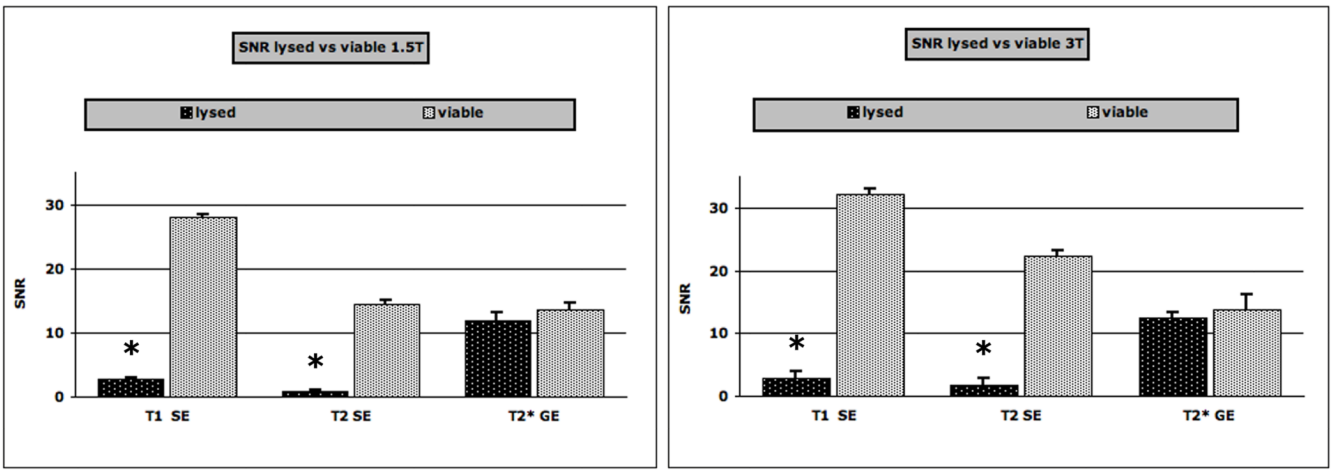

Figure 4.

Signal-to-noise-ratios (SNRs) of viable and lysed Ferucarbotran labeled hMSCs, scanned at 1.5T (left graph) and at 3T (right graph). Data are displayed as means and standard deviations. Note the lower SNR of lysed samples compared to viable hMSCs on T_1 and T_2-weighted SE images (TR 500/ TE 15 and 4000/45 respectively) and the similar SNR of lysed and viable cells on T2*-weighted GE (500/3.7) images. The asterisk indicates a significant difference for SNR between viable and lysed samples.

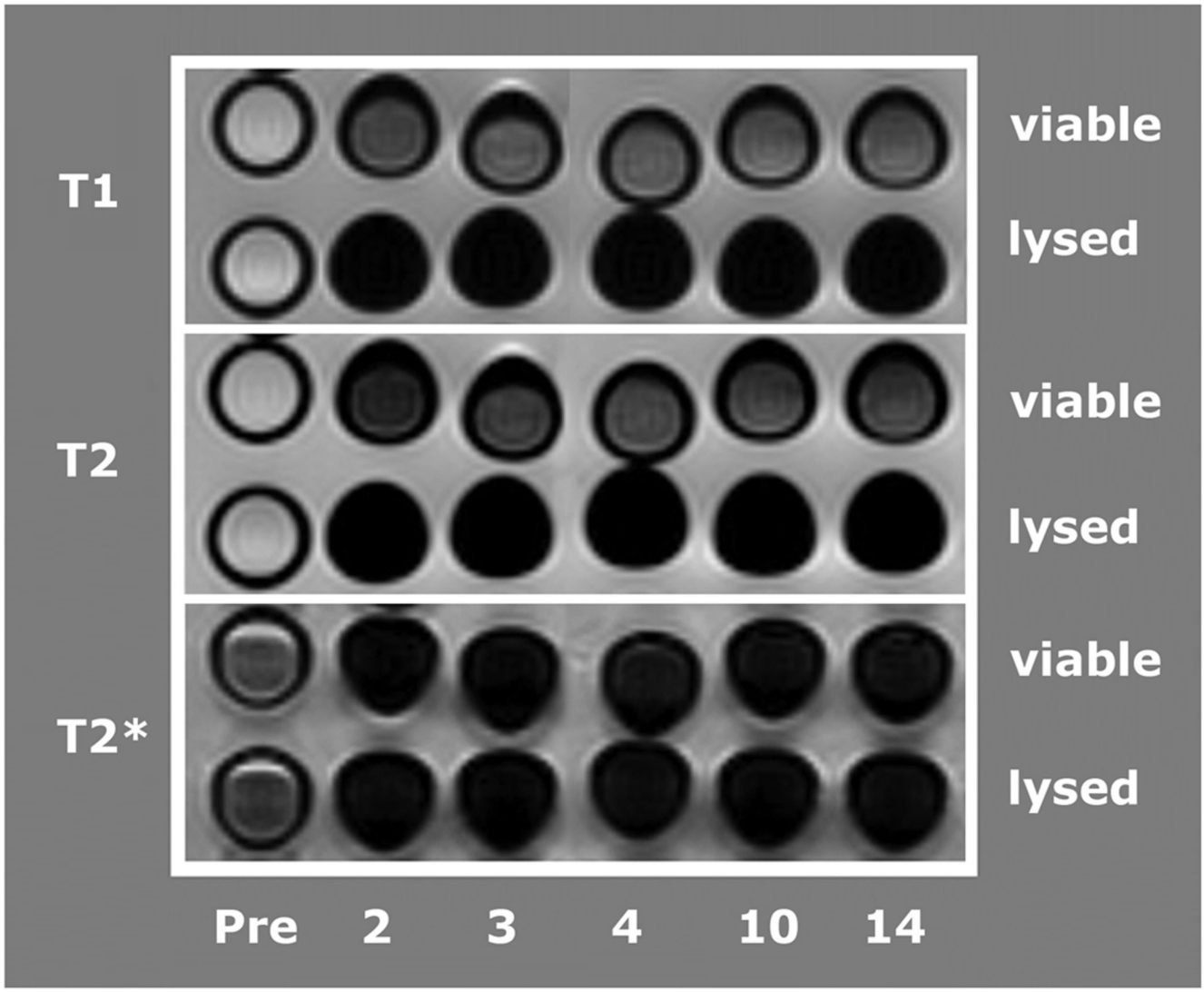

Figure 5.
Axial T_1, T_2 and T_2*-weighted images (Gradient Echo, TE = 7.4, TR = 500 and Spin Echo, TE = 60 ms, TR = 4000 ms) of test tubes with viable Ferucarbotran labeled hMSCs and lysed hMSCs as acquired at 3T. The time scale represents the time interval in between cell labeling and imaging. Notice the marked loss of signal following cell lysis on T_1 and T_2 images but not on T_2* images.